SOLUS | SMART OPTICAL AND ULTRASOUND DIAGNOSTICS OF BREAST CANCER

Project title: Smart Optical and Ultrasound Diagnostics of Breast Cancer

Grant Agreement: 731877

Call identifier: H2020-ICT-2016-1

Topic: ICT-29-2016 Photonics KET 2016

Deliverable 4.5: Performances assessment of optode components

Leader partner: Beneficiary 1, POLIMI

Author(s): Alberto Dalla Mora (POLIMI), Enrico Conca (POLIMI), Vincenzo Sesta (POLIMI), Laura Di Sieno (POLIMI), Alberto Tosi (POLIMI), Alexander Flocke (iCHaus), Simone Tisa (MPD), Antonio Pifferi (POLIMI), Paola Taroni (POLIMI)

Work Package: 4

Estimated delivery: Month 24

Actual delivery: February 6, 2019

Type: Report

Dissemination level: Public

Table of contents

Abbreviations

DCR	Dark Count Rate
DTOF	Distribution of Time-of-Flight
DR	Dynamic Range
FWHM	Full-Width at Half-Maximum
IRF	Instrument Response Function
KPI	Key Performance Indicator
LSB	Least Significant Bit
OCF	Output Current Fine
PC	Personal Computer
PDE	Photon Detection Efficiency
PWC	Pulse Width Coarse
PWF	Pulse Width Fine
RR	Repetition Rate
TCSPC	Time-Correlated Single-Photon Counting
TDC	Time-to-Digital Converter
TW	Time Width

1. Introduction

The aim of this deliverable is the validation of the two most innovative components (integrated circuits) developed in SOLUS: i) the integrated laser driver and ii) the time-gated detector and its timing electronics.

To this purpose, this document reports and discusses the main results of the components characterization. Components specifications were previously defined in D1.1 (Specifications of smart optode components), while their design was presented in D1.3 (First release of integrated driver for pulsed laser diodes) and D1.2 (First release of time-gated detector and timing electronics), respectively.

The report is organized as follows: Section 2 describes the characterization of the integrated laser driver, Section 3 contains the characterization of the time-gated detector and its timing electronics, Section 4 discusses the conclusions.

2. Performance assessment of integrated laser driver

INTRODUCTION

Two test chips were provided by iCHaus, featuring different laser driver output stages, with reference codes TE173Y and TE223. Each of them is capable to drive 2 laser dice. They were both provided coupled to low-cost 980 nm laser dice (U-CP-9850044, Union Optronics Corp., China). The full characterization was performed by POLIMI in collaboration with MPD. Their performance is compared with the first release of driver chips by iCHaus (reference codes TE173 and TE200), which presented some issues as reported in D1.3 (First release of integrated driver for pulsed laser diodes). However, these problems were not affecting the capability to use them for testing the laser pulse shapes and output power.

EXPERIMENTAL SETUP AND DATA ANALYSIS

We performed three different tests on the integrated laser drivers combined to low cost 980 nm laser dice: i) laser pulse shape, ii) laser average output power, iii) laser emission spectrum. In the following, the detail of the measurement setup and data analysis is provided for each case.

LASER PULSE SHAPE

The laser pulse shape was measured with different settings of the drivers, changing: i) the pulse repetition rate (RR), ii) the output current fine regulation (OCF, i.e. the intensity of the current used to drive the laser die), iii) the output pulse width coarse regulation (PWC, i.e. the time duration of the current pulse used to drive the laser die) and iv) the output pulse width fine regulation (PWF). In almost all the cases, at a given RR, the characterization has been performed by looking for the best initial conditions for FOC and PWC, changing the PWF up to when secondary bumps start to be generated after the first peak in the laser pulse shape. The laser pulse shape was measured using a prototype of a compact SPAD module with the following features: i) active area diameter of the CMOS SPAD of 50 μm; ii) IRF (instrument response function) with about 60 ps FWHM and 140 ps tail time constant. Thanks to the embedded time-to-digital converter (TDC), the detector directly provides the histogram of the distribution of time-of-flight (DTOF) of detected photons to a personal computer (PC). As is not possible to focus all the emitted light inside the detector active area due to its small dimension, a thin diffuser (slice of white paper) was placed at about 1 cm of distance from the laser die so as to mix all possible laser emission modes, thus guaranteeing to take into account in the evaluation of the pulse shape of all possible modes which will be injected inside the breast tissue. A circular variable neutral density filter was mounted between the diffuser and the detector in order to adjust the power to fit the single-photon statistics of time-correlated single-photon counting (TCSPC) technique [1]. In order to increase the dynamic range of the acquired waveform, we integrated photons for 5 (15) minutes for measurements performed at 40 MHz (80 MHz) of RR. In post-processing, the constant value of the background noise was subtracted from the DTOF histogram to further increase the dynamic range, thus allowing to evaluate the laser pulse shape over different orders of magnitude.

LASER OUTPUT POWER

Similarly, also the laser output power was measured with different settings of the drivers, i.e. RR, OCF, PWC, and PWF. The power was measured using the S140C power meter (Thorlabs GmbH, Germany). Both the diffuser and the neutral density filter were removed to avoid power losses. Due to the high laser divergence, a short focal length (10 mm) lens was used to focus almost all the emitted light inside the integrating sphere of the power meter.

LASER EMISSION SPECTRUM

The laser emission spectrum was measured with different settings of the drivers, i.e. RR, OCF, PWC, and PWF. The spectrum was measured using the USB2000 spectrometer (Ocean Optics, USA). The diffuser was placed at about 1 cm of distance from the laser die in order to mix all possible laser emission modes, thus guaranteeing to take into account in the evaluation of the emitted spectrum of all possible modes which will be injected inside the breast tissue. The USB2000 measurement input was directly faced to the diffuser. The measured power was adjusted by acting on the distance between the diffuser and the USB2000 measurement input.

RESULTS AND DISCUSSION

Examples of laser pulse shapes obtained at RR = 40 MHz on the second channel of the TE173Y driver (with all the 3 available current outputs connected to the laser die and enabled) are shown in Figure 1, with corresponding laser emission spectra shown in Figure 2. In this configuration it is possible to achieve more than 600 µW of average power without relevant degradations of the laser pulse shape, with 240 ps time width (TW) evaluated as full-width at half-maximum (FWHM). Further, no degradation of the emission spectra can be appreciated by changing the PWF setting. As this is true for all the tested devices, for the sake of synthesis, the spectral figures of merit will not be reported in this document.

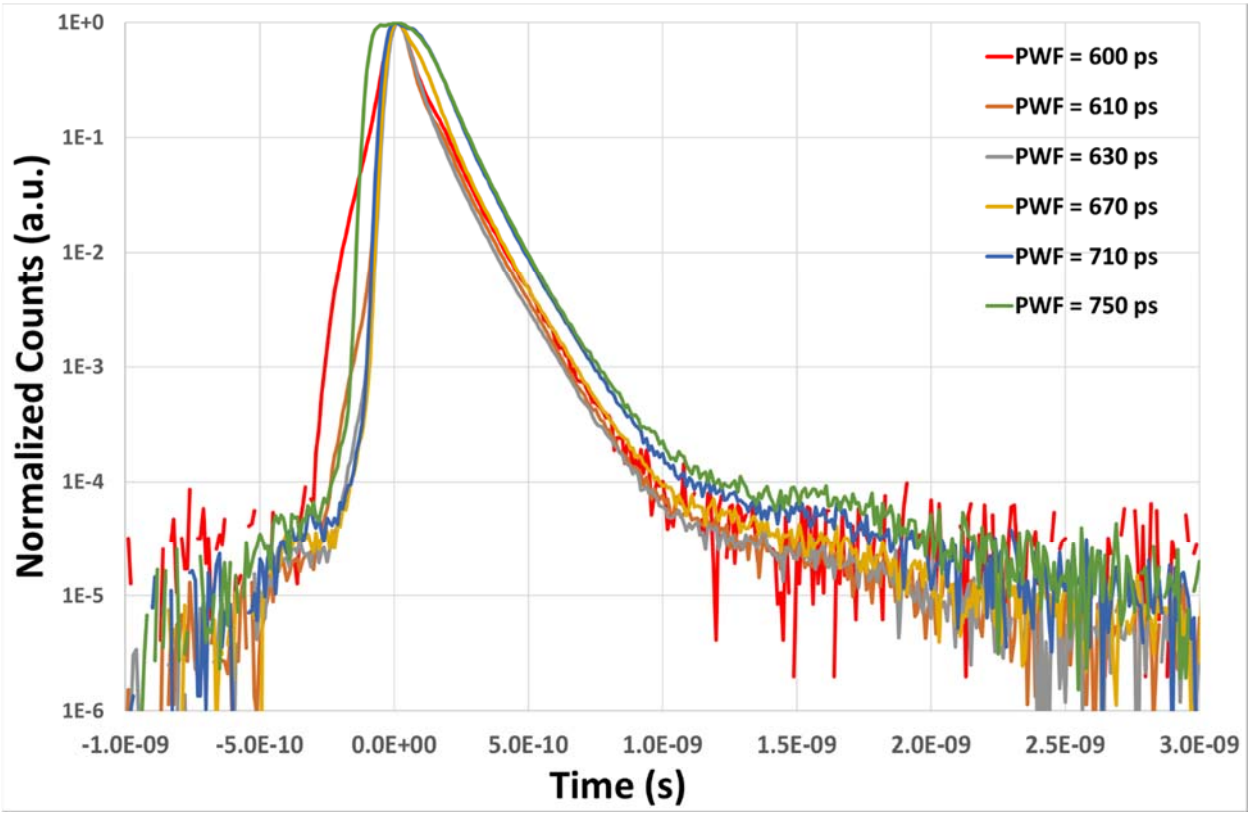

Figure 1 Examples of normalized laser pulse shapes obtained at 40 MHz with the second channel of the TE173Y driver, featuring 3 current outputs enabled, PWC = 100 ps, OCF = 700 mA. The minimum average output power obtained is 0.75 µW (PWF = 600 ps, red line) and the maximum is 626 µW (PWF = 750 ps, green line).

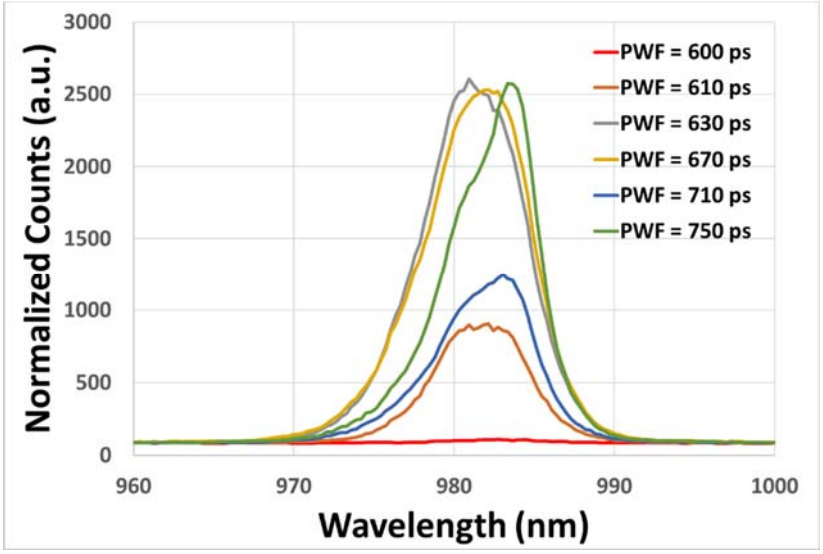

Figure 2 Examples of laser spectra obtained at 40 MHz with the second channel of the TE173Y driver, featuring 3 current outputs enabled, PWC = 100 ps, OCF = 700 mA.

The full characterization data for the TE173Y driver is reported in Table 1 (for channel 1) and Table 2 (for channel 2). Since 3 current outputs are available for each driver, the first column of all tables reports the code of the outputs connected to the laser die (i.e. wire bonded) and enabled. As shown, the connection of all the 3 outputs allows to emit more optical power, without degradation of the pulse width. More than 600 µW can be emitted by keeping the pulse width below 240 ps FWHM.

The full characterization data for the TE223 driver is reported in Table 3 (for channel 1) and Table 4 (for channel 2). In this case, the output power is limited to about 100-150 µW for pulses of FWHM similar to those provided by the TE173Y driver. Generally speaking, these performances can be ascribed to both the laser driver and parasitisms of the laser dice. Thus, even better performances are expected by using the newly developed laser drivers in combination to laser dice more suitable for high power and radiofrequency operations, which have been already selected for SOLUS and are being mounted in the SOLUS optode.

Table 1: Performances of the TE173Y driver (channel 1).

OUTPUTS	PWC [ps]	PWF [ps]	OCF [mA]	RR [MHz]	P [uW]	TW [ps_{FWHM}]
1	588	620	145.27	40	0.56	158
1	588	640	145.27	40	6	106
1	588	680	145.27	40	76	90
1	588	720	145.27	40	118	97
1	588	780	145.27	40	185	155
1	588	820	145.27	40	244	232

Table 2: Performances of the TE173Y driver (channel 2).

OUTPUTS	PWC [ps]	PWF [ps]	OCF [mA]	RR [MHz]	P [uW]	TW [ps_{FWHM}]
1+2+3	100	600	700	40	0.75	105
1+2+3	100	610	700	40	23	87
1+2+3	100	630	700	40	139	89
1+2+3	100	670	700	40	278	123
1+2+3	100	710	700	40	444	184
1+2+3	100	750	700	40	626	240

Table 3: Performances of the TE223 driver (channel 1).

OUTPUTS	PWC [ps]	PWF [ps]	OCF [mA]	RR [MHz]	P [uW]	TW [ps_{FWHM}]
2	832	895	292.16	40	5.4	136
2	832	915	292.16	40	50	99
2	832	955	292.16	40	112	152
2	832	965	292.16	40	128	178
2	832	975	292.16	40	152	247
2	832	985	292.16	40	174	296

Table 4: Performances of the TE223 driver (channel 2).

OUTPUTS	PWC [ps]	PWF [ps]	OCF [mA]	RR [MHz]	P [uW]	TW [ps_{FWHM}]
1+2+3	100	1035	599.46	40	3.5	179
1+2+3	100	1055	599.46	40	50	111
1+2+3	100	1095	599.46	40	120	154
1+2+3	100	1105	599.46	40	150	345
1+2+3	100	1115	599.46	40	174	401
1+2+3	100	1123	599.46	40	191	435

Table 5: Best performances previously obtained at 40 MHz RR with the first release of SOLUS laser drivers (combined with high-performance 830 nm laser die previously selected for SOLUS).

Driver	Channel	OUTPUTS	RR [MHz]	P [uW]	TW [ps_{FWHM}]
TE173	1	2+3	40	1150	200
TE173	2	1+2+3	40	1900	235
TE200	1	2	40	900	170
TE200	2	1+3	40	1550	210

This is also confirmed if comparing the performances with those reported in Table 5, obtained from the previous characterization of the first release of the laser drivers (see D1.3 “First release of integrated driver for pulsed laser diodes”). For instance, with the TE173 driver (featuring the same output stage of the TE173Y) connected to a laser die capable of high power and radiofrequency operation it was possible to obtain 1.9 mW of average power and about 200 ps pulse duration FWHM.

On the TE173Y and TE223, the characterization has been repeated at 80 MHz RR, i.e. the highest targeted laser RR in SOLUS. Results are shown in Table 6. Results at 80 MHz are in line with those at 40 MHz, confirming the better operation of TE173Y driver with all current outputs connected to the laser die. It is worth noting that more than 1 mW and 225 ps FWHM pulse duration are obtained even using an inexpensive laser die, not optimized for high power and radiofrequency operations. The laser pulse shape corresponding to the second channel of TE173Y driver operated at 80 MHz are reported in Figure 3 for two different values of the OCF.

Table 6: Best performances obtained at 80 MHz with the final release of SOLUS laser drivers (combined with inexpensive 980 nm laser die, not optimized for high power operation).

Driver	Channel	OUTPUTS	PWC [ps]	PWF [ps]	OCF [mA]	RR [MHz]	P [uW]	TW [ps_{FWHM}]
TE173Y	1	1	832	711	143.11	80	565	181
TE173Y	2	1+2+3	100	786	600.54	80	1110	224
TE223	1	2	832	960	292.16	80	360	171
TE223	2	1+2+3	100	1055	616.74	80	240	132

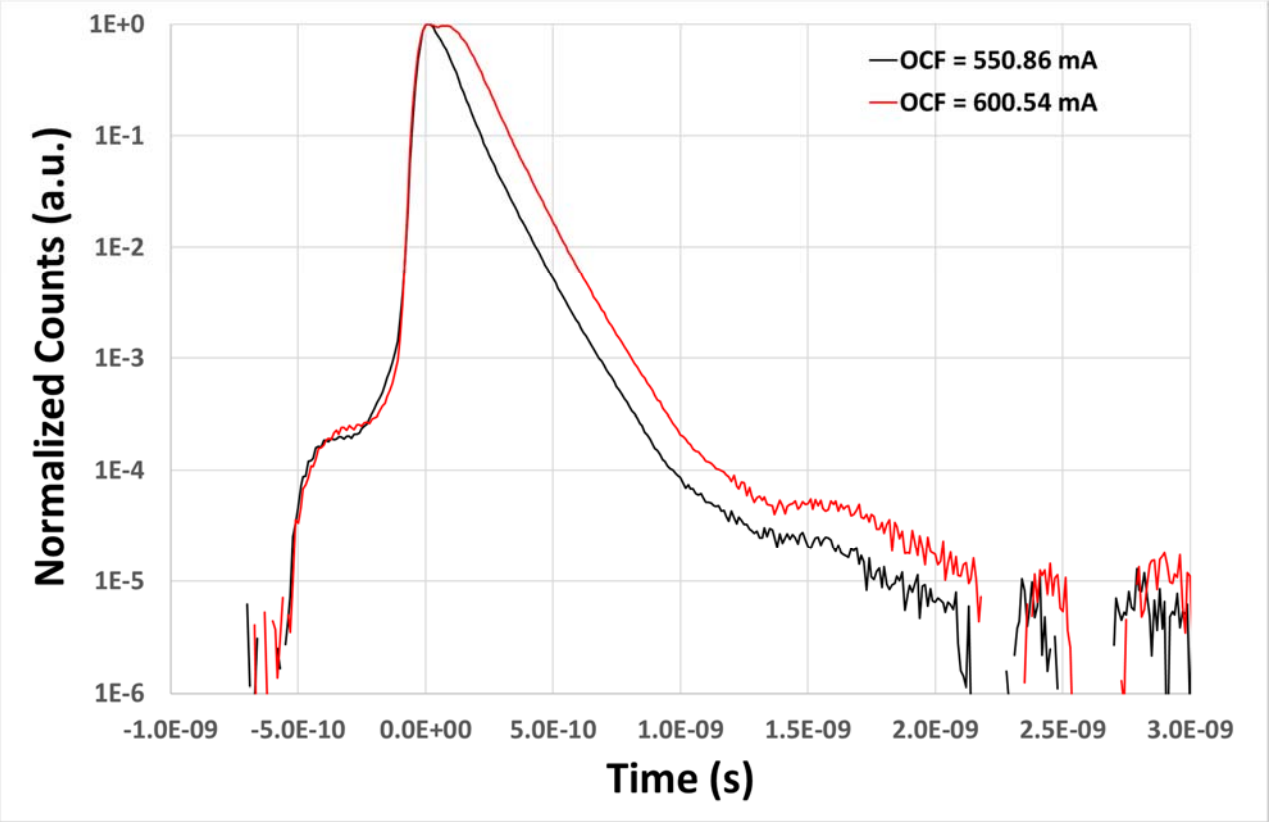

Figure 3 Laser pulse shapes obtained with the second channel of the TE173Y laser driver (3 outputs connected to the laser die and enabled) at two different OCF settings (550.86 mA, featuring 0.54 mW average power and 124 ps FWHM; 600.54, featuring 1.11 mW average power and 224 ps FWHM).

CONCLUSION

In conclusion, the performances of the final releases of the integrated laser drivers have been characterized. In the most suitable configuration, even using a sub-optimal laser die, it is possible to achieve 1.11 mW average power and 224 ps FWHM duration of the laser pulses at 80 MHz repetition rate. Furthermore, 1.9 mW average power and 235 ps FWHM have been measured at 40 MHz using a selected laser die, suitable for high power and radiofrequency operation. These performances are in agreement with specifications defined in D1.1 (Specifications of smart optode components). Moreover, as reported in the Grant Agreement, this deliverable represents the checkpoint for the Key Performance Indicator (KPI) number 1 (source performance at the end of year 2, average power = 1 mW and pulse width (FWHM) ≤ 500 ps"). Hence, with a delay of about 3 months, performances are fully in line with KPI 1.

3. Performance assessment of time-gated detector and timing electronics

INTRODUCTION

A test chip of the time-gated detector (second version) with its integrated timing electronics has been mounted by POLIMI on a test board, thus allowing the experimental characterizations performed by POLIMI and reported here. It was characterized in terms of Photon Detection Efficiency (PDE), Dark Count Rate (DCR), gating performance, temporal response (FWHM, KPI 2), afterpulsing ratio, light harvesting capability of the released detector (i.e. responsivity, KPI 2) and the Instrument Response Function (IRF) shape and dynamic range (KPI 2); the built-in TDC was characterized in terms of single-shot precision, linearity and dead time. Some of these tests (responsivity, IRF, afterpulsing ratio) are based on the Basic Instrumental Performance (BIP) protocol (an internationally agreed protocol devised for the characterization of basic hardware performance of time-domain diffuse optical imagers) [2].

EXPERIMENTAL SETUP AND DATA ANALYSIS

The PDE was measured by means of a calibrated setup consisting of a broadband light source (Quartz Tungsten Halogen lamp) attenuated to the single-photon level, a monochromator, an integrating sphere and a calibrated power meter, which continuously monitors the output power. The detector is placed at a fixed distance from the output of the integrating sphere and the number of output pulses is accumulated by an external counter. The PDE has been measured for a single pixel because, due to the architecture of the chip, the PDE is not affected by the activated area.

The DCR was evaluated on a pixel-by-pixel basis by keeping the detector in dark conditions, enabling one pixel at a time and integrating the number of output pulses during a predefined time interval, then normalizing for the duty cycle and integration time.

The gate window uniformity and the rise time were measured by illuminating the detector with uncorrelated light and collecting the histogram of the arrival times of the output pulses with respect to the electrical gate signal using the TDC integrated in the SOLUS chip.

The temporal response of the detector (FWHM) was measured by a standard TCSPC board (SPC-130, Becker&Hickl GmbH) when illuminated by a pulsed diode laser at 780 nm with a pulse width < 50 ps (FWHM) and a repetition rate of 40 MHz. Its uniformity inside the gate window was measured by moving the pulse time position with respect to the electrical gate signal by means of a picosecond delayer.

The afterpulsing ratio [2] was computed using a laser at 633 nm and with 2 values of enabled active area (1 mm^2 and 6 mm^2).

The characterization of responsivity and IRF shape were done using a state-of-the-art broadband diffuse optical spectroscopy system [3] consisting in a supercontinuum pulsed laser source (repetition rate: 40 MHz). The wavelength selection (in the range 600-1100 nm) was done by means of a prism, whose movement was software controlled. Monochromatic light was then coupled into a 50 µm core fiber and, after an attenuation stage (i.e. u-bracket hosting a stack of variable optical attenuators), it entered a 100 µm core fiber (i.e. injection fiber in case of measurements on phantoms). Photons were then collected by the detector that was directly placed in front of the injection fiber tip (for IRF shape characterization) or in direct contact with the phantom surface (for responsivity measurement). The DTOF of photons was then recorded using a standard TCSPC board (SPC-130, Becker&Hickl GmbH, Germany). Responsivity measurements were carried on using the detector with a gate width set to 10 ns, while for the IRF a gate with of 3 ns was set. In all cases the excess bias was set to 2.9 V.

The responsivity was characterized at 600 nm with different amounts of enabled active area (i.e. 1.06, 2.07, 3.09, 4.01, 5.08, 6.05 and 7.32 mm^2). 1 acquisition of 1 s was recorded for each case. Responsivity was also measured over the wide wavelength spectrum (i.e. from 600 to 1100 nm at step of 50 nm) of interest for SOLUS (“spectral responsivity” in the following). In this case, measurements were carried out turning ON an active area of 7.32 mm^2. As dictated by BIP protocol, for each wavelength 20 repetitions of 1 s each were acquired. The count-rate was set to 1 Mcps above the background noise.

The dynamic range (DR) of the detector was evaluated with acquisitions in a classical IRF configuration (i.e. injection fiber faced to the detector with a thin layer of Teflon in between) using the procedure described in Ref. [4] (i.e. time-gated acquisition). The gate opening of the detector was delayed by means of a home-made delayer over a range of 6 ns at steps of 100 ps. For each delay, one repetition of 1 s was acquired. The measurement was carried out with 4 different values of active area: 1 pixel, 1 mm^2, 3 mm^2 and 6 mm^2. For each active area, measurements were done at wavelengths from 600 nm to 1100 nm at steps of 100 nm. To optimize the reconstruction of the time-gated IRFs (and thus the quantification of the DR, see [4]), the mean value of the background noise (computed on the first delay, where the whole DTOF is recorded) was subtracted to all acquisitions.

The integrated timing electronics was tested using two auxiliary START and STOP inputs of the SOLUS chip. The single-shot precision was measured feeding two signals generated with a pulse generator (rise-time < 3 ns) and the linearity was measured feeding two uncorrelated signals: the START coming from a SPAD module under constant illumination and the STOP coming from the pulse generator.

RESULTS AND DISCUSSION

PHOTON DETECTION EFFICIENCY

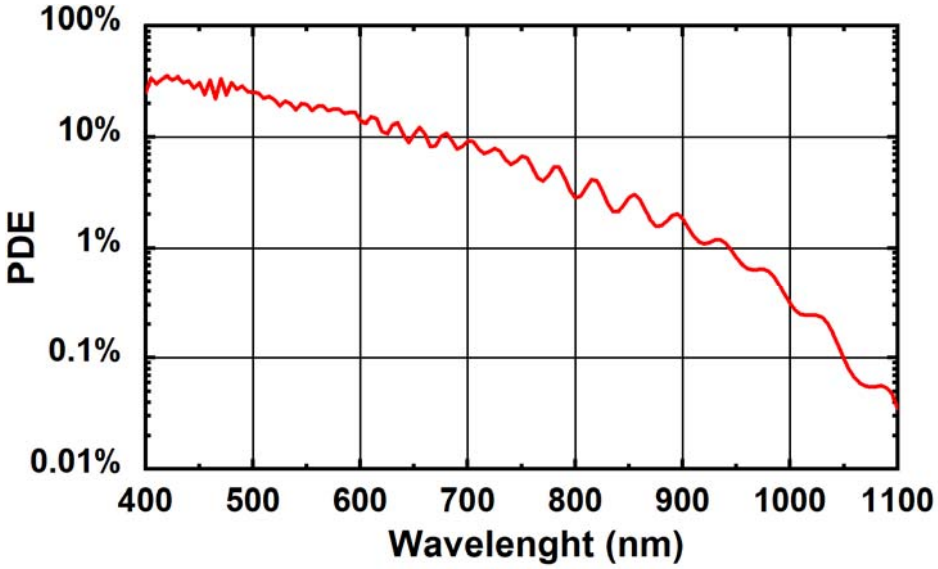

Figure 4 Photon detection efficiency measured at an excess bias of 3.3 V

Figure 4 shows the PDE measured in the range of wavelengths from 400 nm to 1100 nm when the excess bias voltage is set to 3.3 V. These experimental results match the expected values reported in deliverable D1.1 (Specifications of smart optode components).

DARK COUNT RATE (DCR)

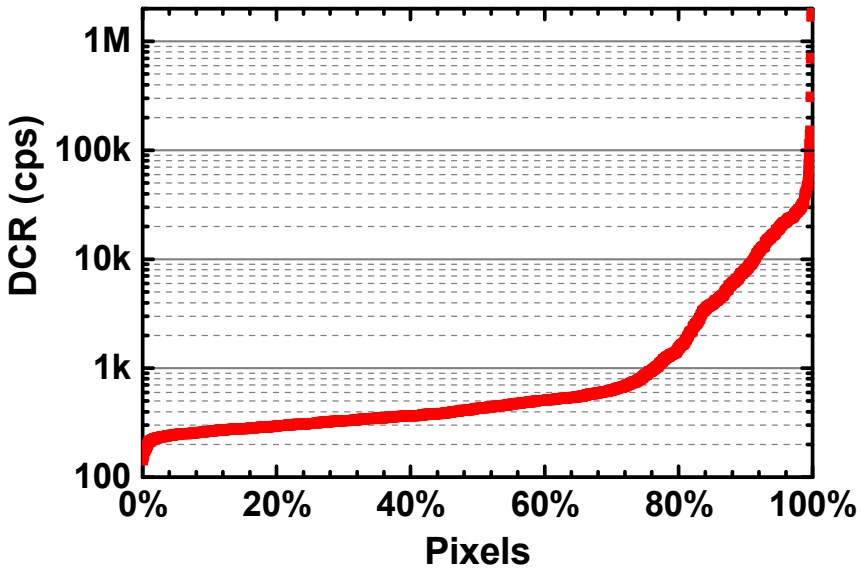

Figure 5 Per-pixel dark count rate distribution over the SOLUS detector.

The DCR for each pixel, sorted in ascending order, is shown in Figure 5. The DCR distribution has a median value of 424 cps per pixel. A change in the slope of the curve can be noticed around 70%, with few extremely hot pixels (DCR > 100 kcps) close to 100%, which can be kept OFF to limit the total DCR of the detector. This total DCR is below the required limit (250 kcps per mm^2, see D1.1 - Specifications of smart optode components -) for active areas as large as 8 mm^2 at room temperature.

GATING PERFORMANCE

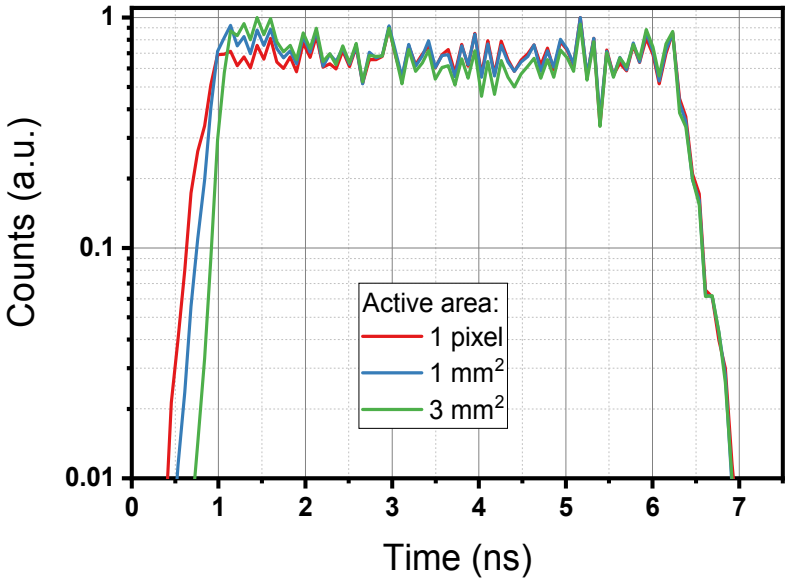

Figure 6 Gate window uniformity for different active areas, as acquired by the integrated TDC and histogram builder.

The histograms of the photon arrival times within the gate window for active areas ranging from one pixel to the target area of 3 mm^2 are shown in Figure 6 when the detector is illuminated with uncorrelated light. Such measurement shows the uniformity of the detector sensitivity inside the gate. The rising edge (20% - 80%) is about 200 ps even for large (≥ 3 mm^2) active areas, thus fully matching the specification of < 1 ns (see D1.1). The gate window is quite uniform up to about 3 mm^2 of active area, while for larger active areas a distortion is present, due to inductive ringing on the connections of the chip power supplies. However, the SOLUS detector still operates correctly in gated mode, properly rejecting early photons arriving before the gate.

TEMPORAL RESPONSE

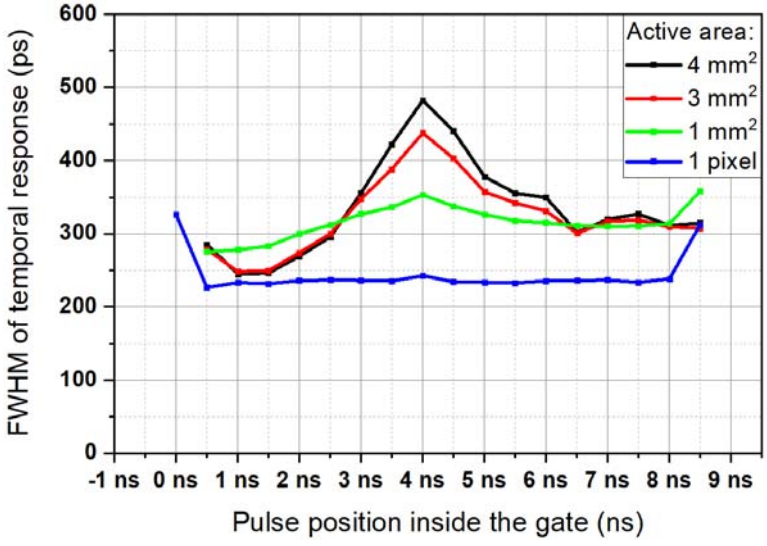

Figure 7 FWHM of the temporal response of SOLUS detector as a function of the position inside the gate window, for various active areas.

The FWHM of the temporal response of the detector as a function of the active area and of the position inside the gate window is reported in Figure 7. The single pixel shows a constant temporal response to the 50 ps laser at all the positions inside the gate window, with a FWHM of ~ 235 ps. The temporal response changes when a wider area of the detector is activated. In detail, a degradation of FWHM is present after 3 ns from the rising edge of the gate window and gets worse as the activated area increases. This is due to the above-mentioned distortion of the gate window. The limit for which FWHM is below

500 ps (in accordance to KPI 2) can be met in all the gate window duration up to about 4 mm^2 of active area, which is still higher than the target area of 3 mm^2. In addition, the FWHM in the first part of the gate window (up to about 2 ns) is < 300 ps for all the selectable active areas.

AFTERPULSING RATIO

The computed afterpulsing ratio is about 5%, without any dependence on the active area.

RESPONSIVITY

Figure 8(a) shows the responsivity as a function of the enabled area at 600 nm. It is worth noting that the responsivity is higher than 10^{-6} m^2sr (as targeted by KPI 2) already for areas larger than about 2 mm^2, approaching 3 times the target when enabling more than 7 mm^2. Figure 8(b) shows the "spectral responsivity" of the detector with a 7.32 mm^2 area. The responsivity is higher than 10^{-6} m^2sr up to 700 nm. As it was expected due to classical trend of photon detection efficiency of silicon detectors (Figure 4), the responsivity decreases for longer wavelength. However, at 1100 nm the responsivity is of the same order of magnitude of best-in-class state-of-the-art instruments [3], where such high values were feasible only switching long wavelengths signal on a different detector optimized for the near-infrared range. In SOLUS, thanks to the wide area of the detector and to the operation without optical fiber on the collection side, similar responsivities at longer wavelengths are thus achieved without the need for a different detector.

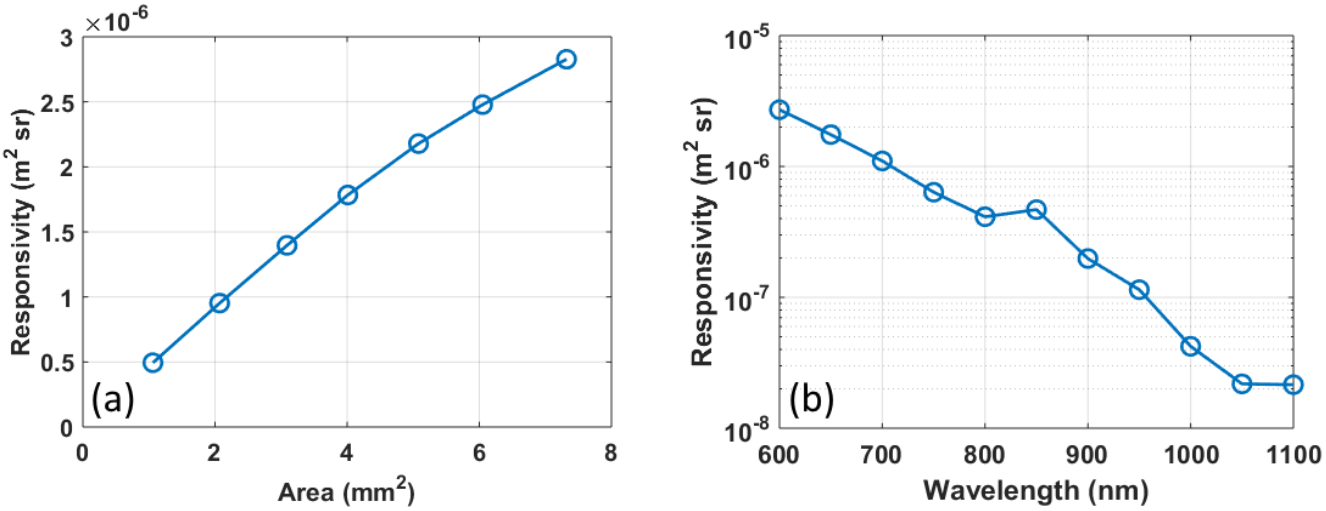

Figure 8 On the left (a), detector responsivity for different values of the active area at 600 nm. On the right (b), responsivity of the same detector computed over the 600-1100 nm range with an active area of 7.32 mm^2.

DYNAMIC RANGE

The reconstructed IRFs acquired for different values of the enabled active area are reported in Figure 9(a). The dynamic range is larger than 5 decades (i.e. 50 dB, as targeted by KPI 2) for all values of the area, thus confirming the homogeneity of the detector in terms of DR. Additionally, the DR does not vary significantly in the 600-1000 nm range (see Figure 9b). The lower DR for the 1100 nm is due to a higher noise floor caused by a well-known spurious emission of the laser used for this characterization in the spectral range close to its pump wavelength (1064 nm).

For both cases, the noise in the reconstruction in the range between 0.8 to 2.2 ns from the IRF peak is only due to a low number of counts in the portion of the curve used in the reconstruction due to the fast decaying behaviour of the detector tail in the timing response, which is highly desired in time-gated acquisitions and does not represent an issue. With an exponential fit of this tail it has been possible to quantify the time constant of its decay, which resulted of about 100 ps, in full agreement with specifications reported in D1.1.

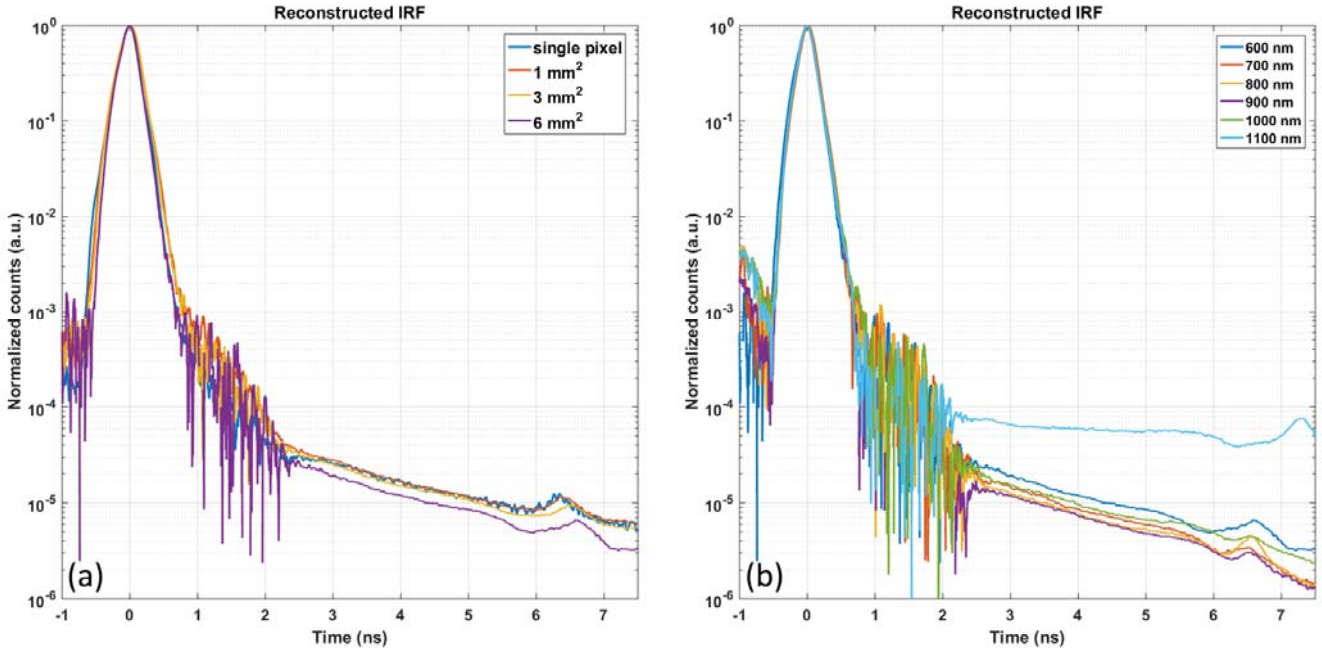

Figure 9 On the left (a), reconstructed IRF for different value of detector active areas measured at 600 nm. On the right (b), reconstructed IRFs acquired with 6 mm² active area at 6 wavelengths.

TIMING ELECTRONICS

The timing electronics has a full scale range of about 10 ns, with channel width (i.e. the LSB, least significant bit) always below about 106 ps. The average LSB is between 76 ps and 78 ps (depending on the sample). The average single-shot precision (measured as FWHM) is 106 ps, with a maximum of 156 ps due to quantization errors. The differential non linearity is about 14% (r.m.s.) of the LSB when the sliding scale is disabled and about 3.9% (r.m.s.) of the LSB with sliding scale enabled.

The dead-time is shorter than 100 ns for the whole TDC range and the histogram can be transferred at a rate up to 30 kHz without additional dead-time between subsequent histograms.

CONCLUSION

In conclusion, the performances of the second release of the time-gated detector with integrated timing electronics have been characterized. In particular, in agreement with specifications defined in D1.1: i) the active area can reach 7.32 mm²; ii) the PDE is ~10% at 700 nm, ~5% at 800 nm, ~2% at 900 nm; iii) the DCR is < 250 kcps/mm²; iv) the timing response exhibits a jitter < 300 ps FWHM (provided that the first 2 ns of the gating window is used) and a diffusion tail time constant of about 100 ps; v) the rising edge of the gating window is about 200 ps even for large (≥ 3 mm²) active areas; vi) the TDC LSB is < 106 ps; the TDC timing jitter is < 156 ps FWHM; vii) the TDC dead time is < 100 ns.

This deliverable represents the checkpoint for the Key Performance Indicator (KPI) number 2 (detection performances at the end of year 2: responsivity > 10^{-6} m² sr, temporal response (FWHM) ≤ 500 ps and dynamic range = 50 dB). In this regard, it has been shown that: i) responsivity can approach a value of $3 \cdot 10^{-6}$ m² sr; ii) the temporal response jitter is < 500 ps over the entire gating windows for active areas up to 4 mm²; iii) the dynamic range of the detector is always larger than 50 dB. Hence, with a delay of about 3 months, performances are fully in line with KPI 2.

4. Conclusions

We reported the results of the characterization of the two main SOLUS basic components, that are the integrated laser driver and the time-gated detector with integrated timing-electronics. Both components have been successfully validated for operating in the SOLUS system. In particular, the laser driver demonstrated the capability to driver laser dice to obtain average optical power of about 2 mW already at 40 MHz of repetition rate (i.e. 2 times the original KPI 1 target) with pulse width lower than 240 ps FWHM (i.e. 2 times better that the KPI 1 target). Additionally, the detector can approach a value of responsivity of $3 \cdot 10^{-6}$ m^2 sr (i.e. 3 times the original KPI 2 target), a temporal response lower than 500 ps in the worst case with active areas up to 4 mm^2 (in line with KPI 2 target) and a dynamic range of more than 50 dB (i.e. in line with KPI 2 target). To conclude, the validated technologies are now suitable for integration in the SOLUS system.

5. References

[1] D. V. O' Connor and D. Phillips, Time-Correlated Single Photon Counting (Academic Press, 1984).

[2] H. Wabnitz, D.R. Taubert, M. Mazurenka, O. Steinkellner, A. Jelzow, R. Macdonald, D. Milej, P. Sawosz, M. Kacprzak, A. Liebert, R. Cooper, J. Hebden, A. Pifferi, A. Farina, I. Bargigia, D. Contini, M. Caffini, L. Zucchelli, L. Spinelli, R. Cubeddu, and A. Torricelli, "Performance assessment of time-domain optical brain imagers, part 1: basic instrumental performance protocol," J. Biomed. Opt. 19, 86010 (2014).

[3] S. Konugolu Venkata Sekar, A. Dalla Mora, I. Bargigia, E. Martinenghi, C. Lindner, P. Farzam, M. Pagliazzi, T. Durduran, P. Taroni, A. Pifferi, and A. Farina, "Broadband (600-1350 nm) Time-Resolved Diffuse Optical Spectrometer for Clinical Use," IEEE J. Sel. Top. Quantum Electron. 22, 7100609 (2016).

[4] A. Tosi, A. Dalla Mora, F. Zappa, A. Gulinatti, D. Contini, A. Pifferi, L. Spinelli, A. Torricelli, and R. Cubeddu, "Fast-gated single-photon counting technique widens dynamic range and speeds up acquisition time in time-resolved measurements.," Opt. Express 19, 10735–46 (2011).